Available online at www.sciencedirect.com
ScienceDirect
Polymer 47 (2006) 6718–6730
polymer
www.elsevier.com/locate/polymer

Effect of clay modifiers on the morphology and physical properties of thermoplastic polyurethane/clay nanocomposites

Cheol Ho Dan [a], Min Ho Lee [a], Young Doo Kim [b], Byong Hun Min [a], Jeong Ho Kim [a,*]

[a] *Department of Chemical Engineering, University of Suwon, San 2-2 Wauri, Bongdameup, Hwasung, Kyunggido 445-743, Republic of Korea*
[b] *Elas Chem Co. Ltd., Yesan, Chugnam, Republic of Korea*

Received 2 February 2006; received in revised form 6 July 2006; accepted 23 July 2006
Available online 10 August 2006

Abstract

Thermoplastic polyurethanes (TPUs)/clay nanocomposites were prepared via melt processing using the ester type and the ether type TPUs and three differently modified organoclays (denoted as C30B, C25A and C15A) as well as pristine montmorillonite (PM). XRD and TEM results showed that the addition of C30B with hydroxyl group led to the nearly exfoliated structures in both TPUs. In the case of C25A and C15A clays, partially intercalated nanocomposites were obtained in both TPUs, where C25A showed better dispersion than C15A. Natural clay (PM) was not effectively dispersed in both TPUs. The tensile properties of nanocomposites with C30B were better than ones with the other clays. Higher tensile properties were obtained for ester type TPU than ether type TPU nanocomposites with all clays tested. Although the improvement in tensile properties decreased after the second extrusion of the nanocomposites, properties of the nanocomposite after first melt processing were still good enough for practical applications. Morphological changes induced by the addition of clays were analyzed using FTIR, DSC and rheological test results. Some clays were observed to cause demixing of hard and soft segments in the nanocomposites and location of clays in either soft segment or hard segment domains was also studied.

Keywords: Polyurethane; Clay; Nanocomposites

1. Introduction

Thermoplastic polyurethanes (TPUs) have been widely used since their inception in the BF Goodrich research laboratories in the 1950s by Schollenberger et al. [1]. TPUs are mainly used in a wide variety of applications such as automotives, screens, roller systems and films, etc. [2]. TPUs are segmented polymers composed of hard and soft segments forming two-phase microstructure. The hard segment is formed by extending a diisocyanate with a low molecular weight diol such as 1,4-butanediol, while the soft segment is composed of hydroxyl-terminated polyester or polyether polyol. In the segmented polyurethanes, phase separation of the urethane hard segments into micro domains has been observed even when the segment length is relatively short, due to the incompatibility of the hard and soft segments. The primary driving force for domain formation is the strong intermolecular interaction between urethane units, which are capable of forming interurethane hydrogen bonds [3–6].

In recent years, polymer/clay nanocomposites have attracted great attention both in industry and academia, since the Toyota group developed clay/nylon 6 nanocomposites with excellent mechanical properties [7,8]. This success has created much attention for the use of clay as a reinforcement material for polymers. These nanocomposites exhibit remarkable improvement compared to the conventional microcomposites in various properties such as mechanical strength, heat resistance, gas permeability, and flammability. So far, polymers such as polyamide, polystyrene, polyethylene, polypropylene, poly (ε-caprolactone), and polyethylene oxide, etc. have been studied in clay-based nanocomposites [9–17].

* Corresponding author. Tel.: +82 31 220 2450; fax: +82 31 220 2528.
E-mail address: jhkim@suwon.ac.kr (J.H. Kim).

0032-3861/$ - see front matter © 2006 Elsevier Ltd. All rights reserved.
doi:10.1016/j.polymer.2006.07.052

Among polymer–clay nanocomposites, some researchers have reported the preparation of polyurethane (PU)/clay nanocomposites by in situ polymerization using organically modified clay showing the improvement in the mechanical properties of those PU/clay nanocomposites [18–28]. However, there are still just a few reports on the thermoplastic polyurethanes (TPUs)/clay nanocomposites. It was reported that the TPU nanocomposites with clay C30B containing hydroxyl functionality exhibit the exfoliated clay dispersion due to the interaction between TPUs and the hydroxyl functionalities resulting in the increase of the mechanical properties [28]. Lately, Pattanayak and Jana [25–27] showed that the exfoliated nanocomposites can be prepared by some unique preparation method resulting in more than 100% increase in tensile strength and modulus along with optical clarity compared to polyurethanes without clay. In the previous studies, mainly pristine montmorillonite (PM) and C30B clays were studied and there were not many dealing with C25A or C15A. Accordingly, in the present study, clays PM, C30B, C25A and C15A with varying degrees of hydrophobicity were used to study the effects of different degrees of polarity or different modifiers on the morphology and properties of nanocomposites depending on the type of polyols in the TPUs such as polyether polyol or polyester polyol. The relationship between the morphology and properties were investigated using FTIR and DSC results.

2. Experimental

2.1. Materials and preparation of nanocomposites

Two types of TPUs were obtained from SK Chemicals: polyether-based TPU (Skythane R185A, $M_w \sim 250{,}000$) and polyester-based TPU (Skythane S185A, $M_w \sim 250{,}000$) having the similar Shore Hardness of 87A. Hard segments of both ether type and ester type TPUs are made of 4,4′-diphenylmethane diisocyanate (MDI) and 1,4-butanediol (BD), but soft segments are different such as poly(tetramethylene oxide) glycol (PTMG, $M_w \sim 1000$) for ether type and poly(butylene adipate) glycol (PBAG, $M_w \sim 1000$) for ester type.

The three types of organically modified clays and natural clays were obtained from Southern Clay Products. Pristine montmorillonite, Cloisite Na^+ (PM), has the cation-exchange capacity (CEC) of 92.6 meq/100 g clay. Organically modified montmorillonite, Cloisite 25A (C25A, CEC: 95 meq/100 g) and Cloisite 15A (C15A, CEC: 125 meq/100 g) are montmorillonites modified with a dimethyl, hydrogenated tallow, 2-ethylhexyl quaternary ammonium ion, and dimethyl, dehydrogenated tallow quaternary ammonium ion, respectively. Cloisite 30B (C30B, CEC: 90 meq/100 g) is a montmorillonite modified with a quaternary ammonium salt having one methyl, one tallow and two $-CH_2CH_2OH$ groups. PM has the highest hydrophilicity and C15A has the lowest, while clay 25A and C30B are located between the two.

TPUs in the form of pellets were dried for 4 h prior to melt blending and clays were dried in a vacuum oven at 80 °C for 12 h. TPUs with different amounts of clays (1, 3 and 5 wt% for all cases and 10 wt% in some cases) were melt-blended in a twin screw extruder (Bautek Corp. BA-19ST) at 190 °C and the extrudate was pelletized. Then, the pelletized nanocomposites were injection molded into specimen for testing in a mini-injection molding machine (Bautek Corp.).

2.2. Characterization

The change in gallery distance of silicate layers in the clay was determined on an X-ray diffractometer (D-8 Advance) using Cu Kα radiation at 40 kV, 35 mA. The samples were scanned at 2°/min. The basal spacing of the clay, d_{001} was calculated using the Bragg's law ($\lambda = 2d \sin\theta$).

TEM images of nanocomposite specimens were obtained using Energy Filtering-Transmission Electron Microscopy (EM-912 Omega, Carl Zeiss Co.) with an operating voltage of 120 kV at the Korea Basic Science Institute. The ultrathin sectioning was performed on an ultramicrotome at −100 °C.

Tensile tests were carried out on a universal testing machine (LR10K Lloyd Instrument), according to ASTM D638 type V method. The crosshead speed was 50 mm/min and at least five measurements were taken.

Fourier transform infrared spectroscopy (FTIR) was performed on FTIR-4200 (Jasco) at a resolution of 4 cm^{-1}. The thermal properties of the nanocomposites were measured by Differential Scanning Calorimetry (DSC, TA Instrument DSC2010). Samples were scanned in nitrogen atmosphere at a heating rate of 20 °C/min. The first-run analysis was conducted by heating the sample from room temperature to 250 °C during which the thermogram was taken for first-run analysis. The second-run analysis was conducted by heating the sample at a heating rate of 20 °C/min from room temperature to 160 °C followed by cooling to −130 °C at a cooling rate of 20 °C/min. Then the second heating run was performed from −100 °C to 250 °C during which the thermogram was taken for the second-run analysis.

The complex viscosity measurement was performed on an MCR 300 with parallel plate geometry of 25 mm in diameter. Dynamic frequency sweep test was conducted at 190 °C with angular frequency ranging from 0.01 to 100 rad s^{-1}.

3. Results and discussion

3.1. Morphology

The polyether-based TPU and polyester-based TPU are hereinafter referred to as ether-TPU and ester-TPU, respectively. Fig. 1(a) shows the X-ray diffraction (XRD) patterns of natural clay PM itself, and nanocomposites of ether-TPU/PM and ester-TPU/PM at 5 wt% clay loadings. In Fig. 1(a), ether- and ester-TPU/PM nanocomposites show d_{001} spacing of 1.32 nm and 1.26 nm, respectively, which is slightly larger than d_{001}-spacing of PM (1.17 nm). This means that the clay PM is not well dispersed in the nanocomposites since there is only a very slight increase in the d-spacing of clays. Rest of the XRD results in Fig. 1 are taken for samples with 5 wt% clay loadings.

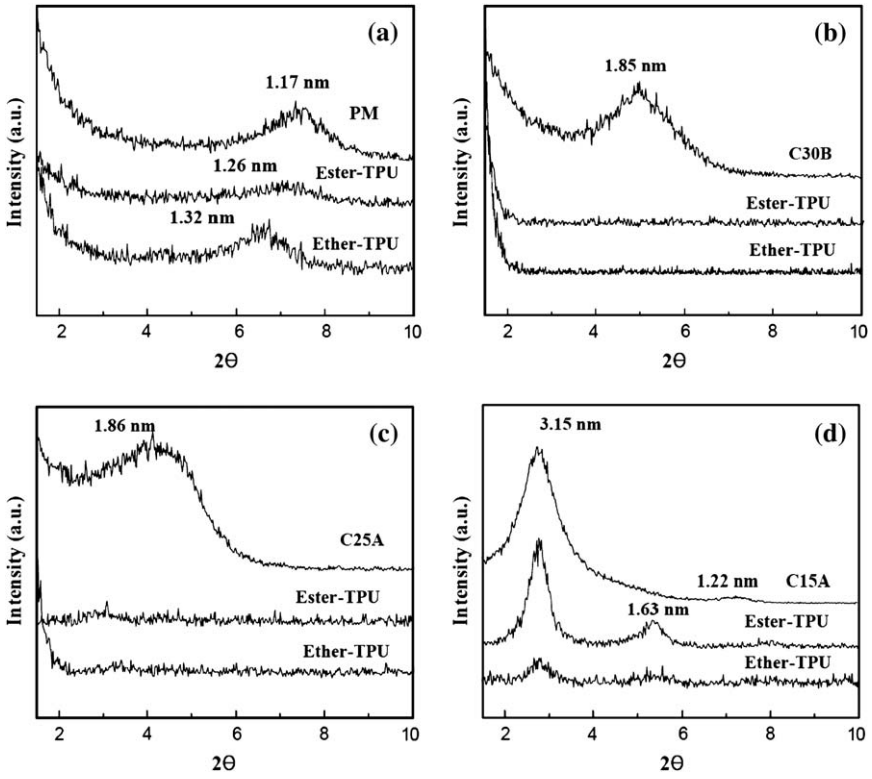

Fig. 1. XRD patterns of ester- and ether-TPUs with 5 wt% of (a) PM, (b) C30B, (c) C25A and (d) C15A.

In Fig. 1(b), the peak of clay C30B itself is shown at $2\theta = 4.8^\circ$ (d-spacing = 1.85 nm). But for nanocomposites with C30B, no peaks are observed for either ether-TPU or ester-TPU. This suggests that silicate layers of C30B are well dispersed in the TPU matrix. The good dispersion of the silicate layers of C30B may be attributed to the specific interaction originated from the hydrogen bonding between carbonyl groups in TPUs and hydroxyl groups in C30B as reported in the previous studies [25–28].

The X-ray diffraction patterns of C25A and TPU/C25A nanocomposites are shown in Fig. 1(c). The ether-TPU/C25A and ester-TPU/C25A nanocomposites exhibit almost no peaks. Judging only from this XRD result, it can be interpreted as the indication of the intercalated or nearly exfoliated clay structures. This is somewhat unexpected since C25A clay does not have any specific functional groups which can be thought to be involved in the specific interaction with TPUs, such as the hydroxyl functionalities in C30B. It is well known that the difficulty in studying the nanocomposites is that no single characterization method can adequately describe the state of clay dispersion in the nanocomposites. The combined analyses are necessary and especially TEM is proved to be quite effective. XRD results are often reported to be misleading in terms of clay dispersion. Therefore, only with the XRD analysis of C25A nanocomposites, it cannot be concluded that these nanocomposites show the intercalated or the exfoliated clay structures. In this regard, TEM pictures were taken and the results are discussed in conjunction with the XRD results later in this section for all the nanocomposites including those with C25A and C30B. Fig. 1(d) shows X-ray diffraction patterns for C15A itself, nanocomposites of ether-TPU/C15A and ester-TPU/C15A. In this Fig. 1(d), ester-TPU nanocomposite shows sharp peaks at $2\theta = 2.8^\circ$ (d_{001} spacing of 3.15 nm), same as that of C15A, while the peak of ether-TPU is smaller at the same 2θ. A weak peak appears at $2\theta = 7.25^\circ$ ($d = 1.22$ nm) in the clay C15A, while ether-TPU and ester-TPU nanocomposites show corresponding peaks at $2\theta = 5.3^\circ$ and 5.4° (d_{002}-spacing = 1.66 nm and 1.63 nm), respectively. Although it is ambiguous if the decrease in the peak intensity of 2θ of d_{001} peaks can be related to a change in the degree of clay dispersion, the increase in the d_{002} spacing of ether- and ester-TPU nanocomposites may indicate that some changes in the C15A platelets have occurred in these nanocomposites.

To confirm the XRD results and clearly see the dispersion state of clays in the nanocomposites, TEM pictures were taken as described above. The TEM images of the ester-TPU/clay nanocomposites with 5 wt% clay loadings are shown in Fig. 2. In the TEM images for the ester-TPU/PM nanocomposites (Fig. 2(a)), thick agglomerated clay particles are observed indicating very poor dispersion of clay. Fig. 2(b) shows clay dispersion in the ester-TPU/C30B nanocomposites. In both the 500 nm scale image and the 50 nm one (inset), platelets of clay C30B are observed to show dispersions close to exfoliation. In the 50 nm scale image, two- or three-layered clays are observed. This state of clay dispersion is close to that of the clay in the nanocomposites prepared by in situ polymerization though it does not completely reach the same level [25–27]. This result shows that very good dispersion of clay

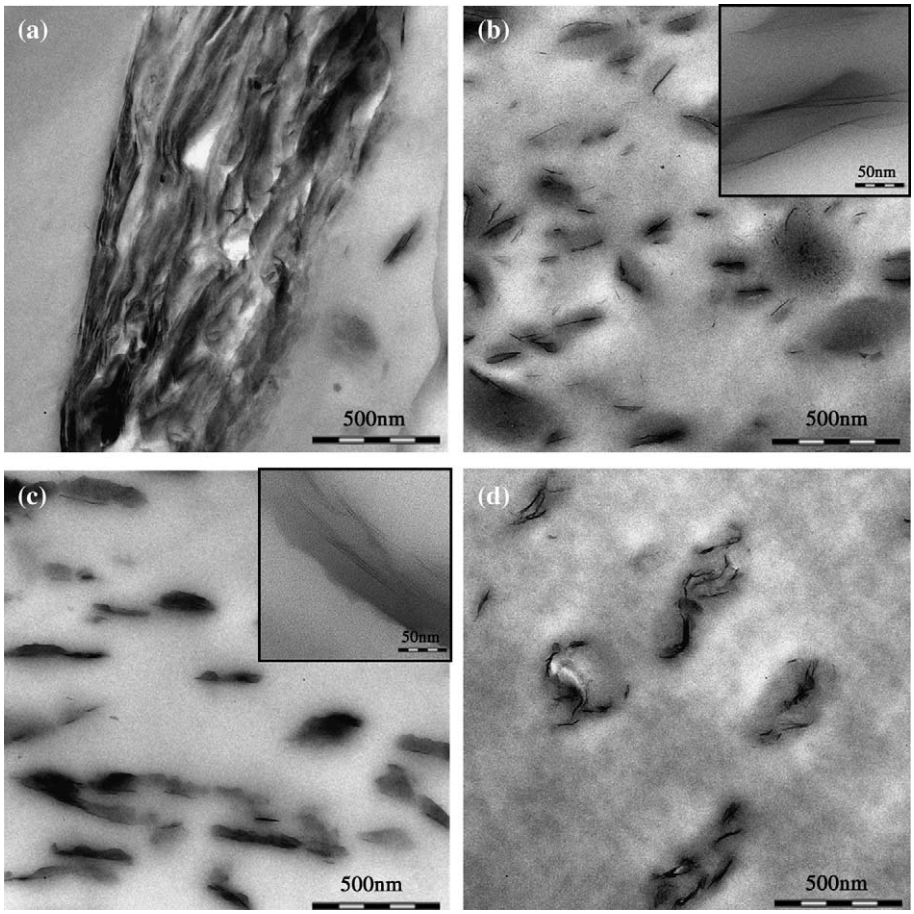

Fig. 2. TEM images of ester-TPU nanocomposites with 5 wt% of (a) PM, (b) C30B, (c) C25A, and (d) C15A.

can be achieved even by melt blending in the twin screw extruder in case of C30B. As explained above, the driving force for the exfoliation of clay layers of C30B is believed to result from the polar interactions between the carbonyl groups present in TPU and the hydroxyl groups existing in the C30B employed in this study. This observation is in agreement with our previous XRD results. In the image of ester-TPU with clay C25A in Fig. 2(c), platelets of C25A are observed to be well dispersed in the TPU matrix, though not exactly comparable to C30B. Especially, from the 50 nm scale TEM image (inset) of this nanocomposite, the distance between the silicate layers of C25A in ester-TPU was measured to be around 2.8 nm, which is larger than the original C25A silicate layer distance of 1.85 nm indicating that C25A clays in these nanocomposites were intercalated by ester-TPU. These results are well correlated with the XRD results where almost no peaks were observed for ester-TPU/C25A nanocomposites. Also from the inset picture, the number of clay layers in one clay particle is observed to be around three to five, which is a little larger than C30B cases, but still much smaller than PM nanocomposites. TEM images of nanocomposite of ester-TPU/C15A are shown in Fig. 2(d), where the degree of dispersion of clay is observed to be better than ester-TPU/PM, but a little poorer than TPU/C25A case. This is in agreement with the XRD result that some changes in clay layers were expected.

The TEM images of ether-TPU/clay nanocomposites shown in Fig. 3 generally exhibit the similar trend as the ester-TPU nanocomposites. The clays are not dispersed well in ether-TPU with PM as shown in Fig. 3(a). For ether-TPU/C30B nanocomposites (Fig. 3(b)), the clay layers of C30B are shown to be uniformly dispersed in the TPU matrix close to exfoliation. This result suggests that effective entry of TPU chains into the silicate layers of C30B leads to a fairly good exfoliation of silicate layers. In comparison with ester-TPU/C30B in Fig. 2(b), TEM images of ether-TPU/C30B shows better clay dispersion in the matrix TPU. In the image of ether-TPU/C25A (Fig. 3(c)), fairly good clay dispersion was observed as in ester-TPU/C25A nanocomposites, though far from ether-TPU/C30B cases. Comparing the clay dispersion of ether-TPU/C25A to ester-TPU/C25A, it is hard to tell which shows the better dispersion, although the length of clay particles in ester-TPU/C25A nanocomposites is a little shorter. In the TEM picture of ether-TPU nanocomposites with C15A (Fig. 3(d)), the dispersion of clay looks similar, but ether-TPU/C25A case is observed to be slightly better. Better clay dispersion in C25A nanocomposites compared to C15A even without any specific functional group present in C25A, such as the hydroxyl group in C30B, may be explained in the thermodynamic sense that the balance between platelet spacing caused by the modifier, level of access to exposed

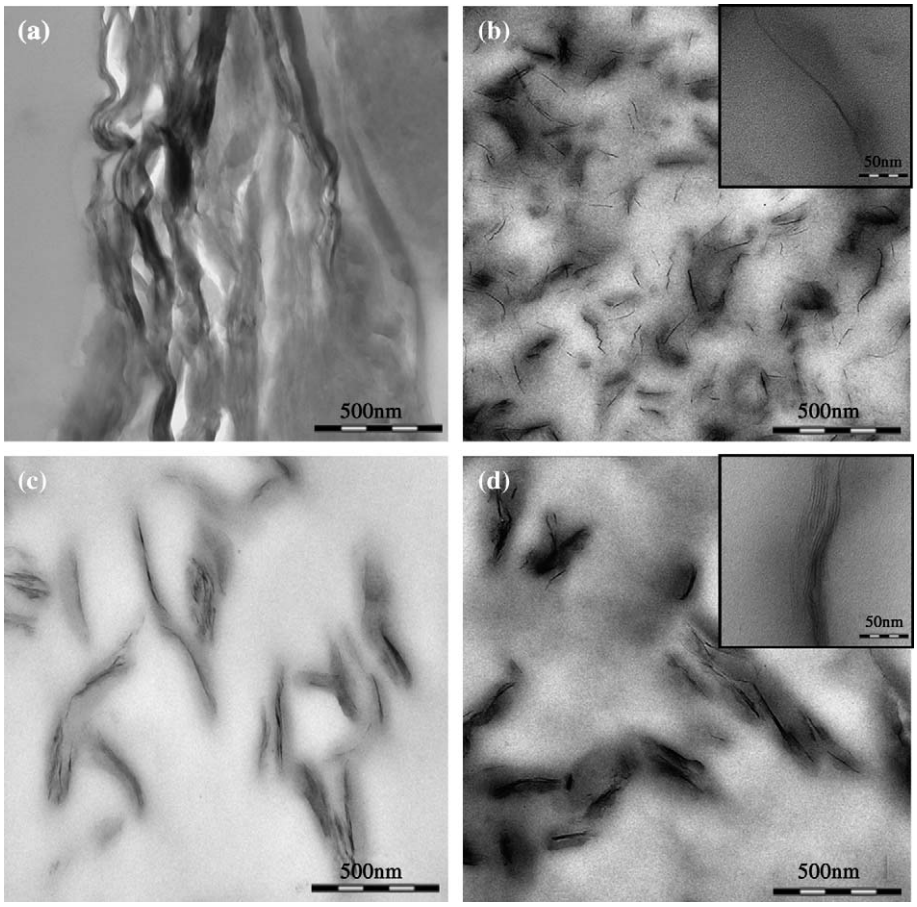

Fig. 3. TEM images of ether-TPU nanocomposites with 5 wt% of (a) PM, (b) C30B, (c) C25A, and (d) C15A.

silicate surface and the number of unfavorable interactions between the polymer and the alkyl units of modifier play the important role as proposed by Fornes et al. [29]. In that paper, the properties of clay surface were explained in terms of contribution from silicate surface of original clay exposed to polymers as well as from the organic modifier. In the case of C30B, it has the hydroxyethyl groups in the clay modifier, and it is expected that this clay can be dispersed well in the TPUs through hydrogen bonding. But in the case of C25A or C15A, there are no functional groups that can cause some specific interaction with the TPUs. Above XRD and TEM results showed a fairly good dispersion of C25A in the TPU matrix while the clay dispersion of the C15A nanocomposite was not that good compared to C25A cases. The difference between C25A and C15A is that C15A has longer alkyl chain at one branch of quaternary ammonium ion in the modifier than C25A and also, C15A has a larger modifier concentration than C25A. This means that C15A has more modifiers so that more clay surface may be covered by some excess modifiers that may be present at the clay surface. Although there is a report in the literature that the modifiers existing in excess of the ion exchange capacity of natural clay (PM) reside primarily in the interlayer, not on the outer surface of clay [30], the possibility that some of the excess modifiers can still exist outside the surface of the clay cannot be excluded completely, especially when the excess amount is significant such as 15A (125 meq/100 g clay) in this study. In this case, majority of the outer surface of the clay can be covered by the hydrophobic modifier and the affinity of the modified clay with TPUs may become weak. Clay 15A may be regarded as almost hydrophobic in nature since only a small part of pure inorganic clay surface may be exposed to polymer. Clay 25A has about the same ion exchange capacity (95 meq/100 g clay) with PM (92.6 meq/100 g clay) and probably does not possess much excess modifier than C15A, although there may be still some unexchanged Na^+. This may leave some surface of the hydrophilic clay exposed to polymer and the balance of this hydrophilic surface and the hydrophobic modifier makes C25A more similar to the nature of ester- or ether-TPUs, which may explain the fairly good dispersion of C25A especially in the ester-TPUs. This may be another manifestation of the reports that interaction between clay and polymer can be more important than that between modifier and polymer in the clay dispersion [31,32]. Of course, the modifiers in both C25A and C15A increase the gallery height and make the layer separation much easier by shear from extruder since the modifier inside the layer weakens the electrostatic force between silicate layers compared to PM, which may partly explain the better clay dispersion in C15A nanocomposites compared to PM nanocomposites.

3.2. FTIR and DSC analyses

3.2.1. Ether-TPU nanocomposites

Fig. 4(a) and (b) exhibits FTIR spectra of ether-TPU and ester-TPU along with the ones containing 5 wt% C30B, respectively. In Fig. 4(a) of ether-TPU, the −NH absorption peak is observed at 3325 cm^{-1} which is due to the hydrogen bonded −NH in the urethane linkage, while carbonyl −C═O stretchings are shown at 1730 cm^{-1} and 1701 cm^{-1} which are considered to be free and hydrogen bonded carbonyls, respectively. The −NH peak of ester-TPU is located at 3332 cm^{-1} as shown in Fig. 4(b) and −C═O peaks are at 1728 cm^{-1} and 1703 cm^{-1}. Usually, the carbonyl peaks around 1700 cm^{-1} are irresolvable due to the superposition of peaks from urethanes and ester-polyols. In some cases, two peaks are observed [33] and the ones for ester-TPUs in this study are considered to be from carbonyls of urethanes and ester-polyols.

Typically the −NH groups in the urethane linkage form hydrogen bonds with carbonyls of the urethane linkage in the hard segment in both cases of ether-TPU and ester-TPU. The −NH groups are also able to form hydrogen bond with ether oxygen of ether-polyol in the soft segment in case of ether-TPU and with carbonyl of ester-polyol in the soft segment in case of ester-TPU. Therefore, careful examination of −NH and carbonyl peaks in the FTIR spectra can give some information on the morphology of the hard and soft segments in the polyurethane as done by Pattanayak and Jana [25–27]. In this regard, the ratio of area under the peaks of −NH (A_{NH}) and that of −CH (2860–2940 cm^{-1}) (A_{CH}) was calculated and shown in Table 1. The area under −CH stretching was used as the internal standard. Also included in Table 1 is the ratio of areas under hydrogen bonded carbonyl peaks (A_{HCO}) and free carbonyl peaks (A_{FCO}) for ether-TPU nanocomposites. The ratios in the Table 1 are average values from five measurements and the range of deviation of measured values from the average values is ±0.001 for A_{NH}/A_{CH} of ether-TPU/clays. The deviation varies in other cases depending on the type of clays added: for all other cases, ±0.01 for nanocomposites with PM and C30B as well as neat TPUs, and ±0.02 for the ones with C25A and C15A.

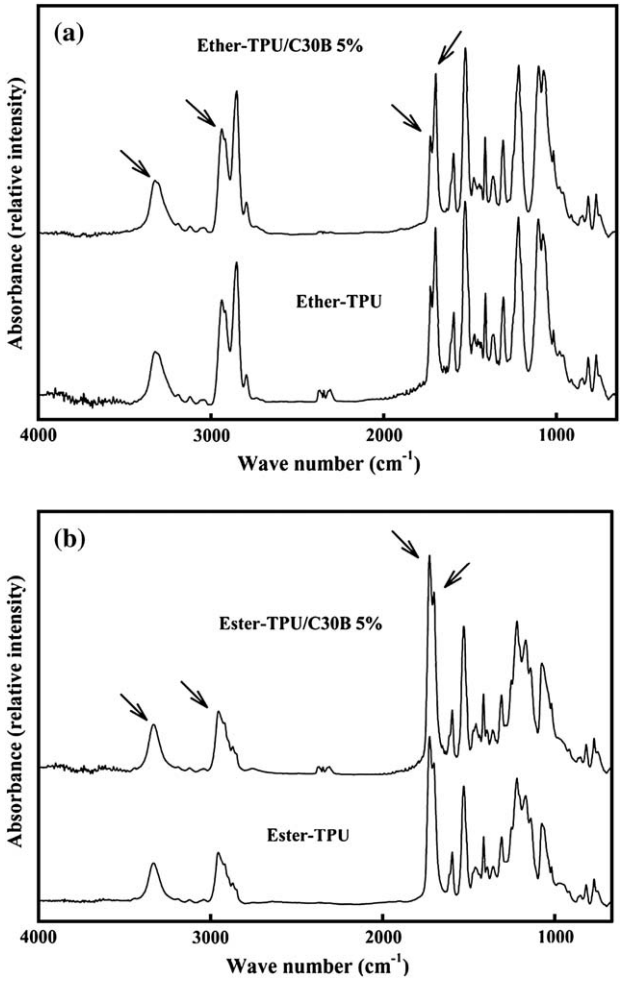

Fig. 4. FTIR spectra (a) of ether-TPU and its nanocomposite with 5 wt% C30B, and (b) of ester-TPU and its nanocomposite with 5 wt% C30B.

In the nanocomposites of ether-TPU with PM, the ratio of A_{NH}/A_{CH} (0.31) remains almost the same as that of pure ether-TPU (0.32) as shown in Table 1, while the ratio of hydrogen bonded carbonyl and free carbonyl (A_{HCO}/A_{FCO}) for ether-TPU/PM increased to 2.61 from 2.41 of pure ether-TPU. This increase in A_{HCO}/A_{FCO} value was unexpected, since clay PM was thought not to give much effect on the TPU matrix. But the change in FTIR spectra may originate not only from the interaction between the clay and the TPUs but also from the morphology change induced by clay addition. Therefore, the FTIR results need to be considered along with other analyses that can give some information on the morphology. In this context, TPU nanocomposite samples were tested by differential scanning calorimetry. Fig. 5(a) shows the DSC results obtained from the first run of ether-TPU nanocomposites scanned from room temperature to 250 °C. In the thermogram, two endothermic peaks appear in the region around 80 °C and 160 °C which are ascribed to the disruption of short range order induced by room temperature annealing and disordering of better ordered hard segment domains, respectively, as reported in the previous study [34]. The area under the endothermic peak around 160 °C may be considered as the manifestation of the amount of the hard segment domains or the level of ordering in the hard segment domains. Those areas of 160 °C endothermic peaks for ether-TPU nanocomposites are summarized in Table 2 along

Table 1
Ratio of the areas under the specific peaks

	Ether-TPU		Ester-TPU
	A_{NH}/A_{CH}	A_{HCO}/A_{FCO}	A_{NH}/A_{CH}
TPU	0.32	2.41	0.62
TPU/PM (5 wt%)	0.31	2.61	0.62
TPU/C30B (1 wt%)	0.31	2.41	0.65
TPU/C30B (3 wt%)	0.31	2.45	0.65
TPU/C30B (5 wt%)	0.31	2.47	0.65
TPU/C25A (5 wt%)	0.31	2.45	0.58
TPU/C15A (5 wt%)	0.29	2.45	0.46

A_{NH}: area under the hydrogen bonded −NH peak; A_{CH}: area under the −CH stretching peak; A_{HCO}: area under the hydrogen bonded −C═O peak; A_{FCO}: area under the free −C═O peak.

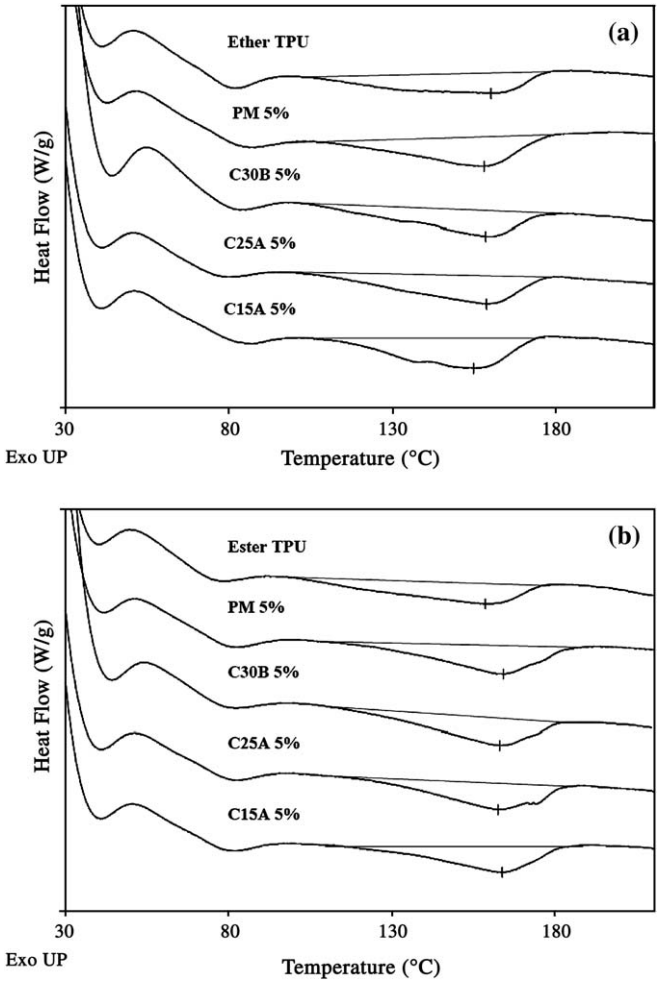

Fig. 5. DSC thermograms of nanocomposites of (a) ether-TPU and (b) ester-TPU (first-run results).

with the corresponding data for ester-TPU nanocomposites shown in Fig. 5(b). Table 2 shows that the endothermic peak area (8.34) of ether-TPU/PM is fairly larger than that (7.44) of neat TPU, which means that PM did give some effect on the morphology of TPU/PM nanocomposites. Since more ordering in the hard segment domains may increase this peak area, clay PM appears to promote the ordering in hard segments and demixing of soft and hard segments which may be the reason for the above increase in the ratio of A_{HCO}/A_{FCO} from 2.41 to 2.61 in FTIR. Demixing or more ordering in the hard segments is reported to cause the higher interurethane hydrogen bonding and lowering of urethane–ether hydrogen bonding [34]. Higher interurethane bonding between

Table 2
Area under the endothermic peak around 160 °C from the first-run DSC results

	Ether-TPU nanocomposites (J/g)	Ester-TPU nanocomposites (J/g)
TPU	7.44	7.35
TPU/PM (5 wt%)	8.34	8.10
TPU/C30B (5 wt%)	7.19	7.22
TPU/C25A (5 wt%)	8.28	7.27
TPU/C15A (5 wt%)	8.98	7.05

–NH and carbonyl increases A_{HCO}/A_{FCO} ratio. Since PM is hydrophilic in nature and has some structural hydroxyl groups, clay PM may interact with hard segments which may also contribute to the increase in the ratio of A_{HCO}/A_{FCO}, although the possibility of inclusion of PM in soft segment domains cannot be ruled out completely.

To check the effect of clays on the soft segment domains using DSC, nanocomposite samples were heated from room temperature to 160 °C and then cooled to −130 °C at a rate of 20 °C. After this, DSC thermograms were taken by reheating at 20 °C/min, of which the results (the second-run result) for ether-TPU nanocomposites are shown in Fig. 6(a). DSC thermograms for all samples exhibit exothermic peaks around −60 °C, which may arise from movement of soft segment polyols. The onset temperature of this exothermic peak for neat ether-TPU appears around −72 °C. Corresponding peaks for ether-TPU/PM show the same onset temperature, which means that PM did not give much effect on the soft segment polyols. This supports that PM may interact with hard segments of ether-TPUs.

In ether-TPU/C30B, the value of A_{NH}/A_{CH} in Table 1 remains about the same as pure TPU and that of A_{HCO}/A_{FCO} increased up to 2.47 at 5 wt% C30B loading from 2.41 of neat TPUs. For C30B nanocomposites, data for 1 wt% and 3 wt%

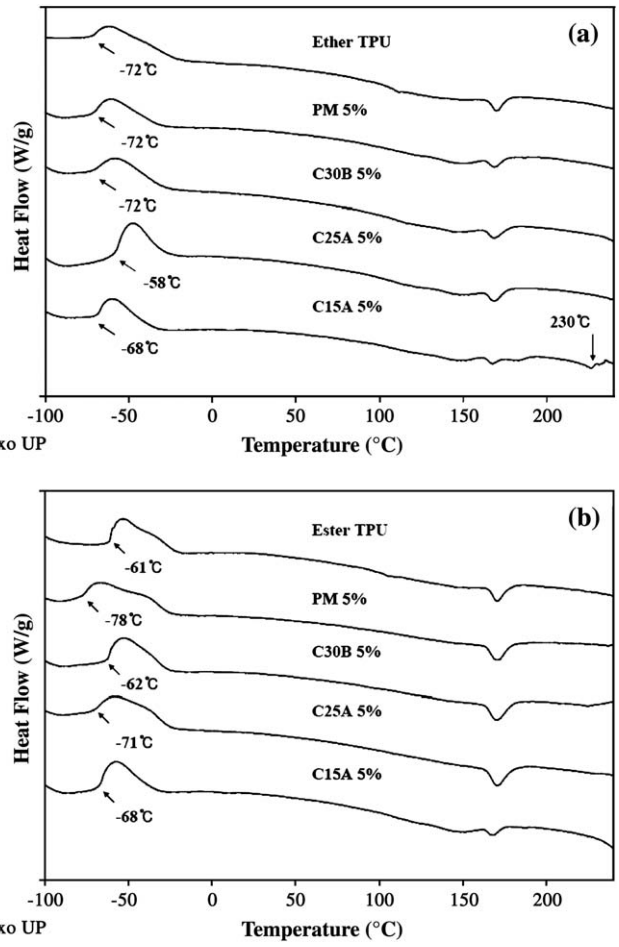

Fig. 6. DSC thermograms of nanocomposites of (a) ether-TPU and (b) ester-TPU (second-run results).

clay loadings were also included in Table 1. More increase in A_{HCO}/A_{FCO} value was observed with increasing C30B amount, which suggested that C30B may be involved in the interaction with ether-TPUs or in the morphology change. In C30B nanocomposites, the hydroxyls (−OH) in the modifier of clay C30B may form hydrogen bonding with the free carbonyls in the hard segment or the ether oxygen in the soft segment. In the former case, it may lead to the increase in the value of A_{HCO}/A_{FCO} which may explain the above FTIR result. This kind of interaction between carbonyls and hydroxyls of C30B was already mentioned in the previous study by Pattanayak and Jana [25]. In the DSC results of Table 2, endothermic peak area (7.19) for C30B nanocomposites is rather lower than that (7.44) of neat ether-TPU, though the difference is small. This means that ordering in the hard domains became slightly less in ether-TPU/C30B than in neat TPU, which may support the above consideration that some of the hydroxyl groups in C30B may interact with carbonyls in the hard segments resulting in slightly less ordering of hard domains. This is manifested in the TEM images where the dispersion of clay C30B is very good through all the phases. With less ordering in the hard segment phases, the interurethane hydrogen bonding may become weak and the decrease in the hydrogen bonded −NH intensity is expected in the FTIR spectra. But the change in ordering is quite small as can be seen from the small change in endothermic area and also if there is any −NH loosened from less ordering, some of them can form hydrogen bonding again with ether oxygen in the soft segments. Both cases will maintain the hydrogen bonded −NH intensity almost unchanged from that of neat TPUs. The onset temperatures of the soft segment exothermic peak in Fig. 6(a) for neat ether-TPU and ether-TPU/C30B were observed to be about the same around −72 °C, which means that C30B changes little the morphology of soft segment phases.

In the previous study of the similar system [27], it is reported that this A_{HCO}/A_{FCO} ratio for the ether-TPU/C30B becomes lower than that of neat TPU, while the increase is observed in the present study. This may arise from the different morphologies between the two studies since the different mixing methods such as different mixing equipment and different mixing temperature, and TPUs with different specifications were used resulting in different clay dispersion. One thing to be noted is that in both studies the value of A_{HCO}/A_{FCO} increases with increasing C30B contents regardless of the absolute value of the A_{HCO}/A_{FCO} ratio.

In the nanocomposites of ether-TPU/C25A, the ratio of A_{NH}/A_{CH} remains again almost the same as that of pure ether-TPU, while the ratio of A_{HCO}/A_{FCO} increased a little to 2.45 from 2.41 of pure ether-TPU. The slight increase in A_{HCO}/A_{FCO} value in this case cannot be considered to be due to the same reason as in C30B nanocomposite case, since there is no hydrogen bonding site available in C25A, such as hydroxyls in C30B.

The endothermic area (8.28) of ether-TPU/C25A from DSC results in Table 2 is larger than that (7.44) of neat ether-TPU. This means that the size of the hard domain or the ordering in the hard domain increased for C25A nanocomposites compared to neat ether-TPU. In C25A nanocomposites, clay C25A may induce the demixing of hard and soft segments since C25A is somewhat hydrophobic in nature and it prefers to be with ether-polyols than with urethane segments. This means that some of the urethane segments originally dispersed in the soft polyol phase rearranged themselves into the hard segments resulting in more ordered hard segments. Since some of the urethane chains which were originally forming hydrogen bond with the ether oxygen of soft segments moved to hard segments, the number of hydrogen bonding between −NH and ether oxygen decreased. But since the −NH group moving to hard segments are now forming hydrogen bond with free carbonyls of the urethane linkage in the hard segments, A_{NH}/A_{CH} value remains around the same, while the value of A_{HCO}/A_{FCO} increased due to more carbonyls involved in hydrogen bonding. Possibilities cannot be ruled out completely that some of the structural hydroxyls in C25A surface form hydrogen bonding with −NH in the hard segment, which also contribute a little to the −NH hydrogen bonding intensity in FTIR spectra.

In the same context, there may be also demixing of hard and soft segments and ordering of hard domains in the ether-TPU nanocomposites with C15A which has some more excess aliphatic modifiers, resulting in more demixing and more ordering of hard domains than C25A nanocomposites. Actually, the endothermic area (8.98) of ether-TPU/C15A from the DSC results in Table 2 is even larger than that of ether-TPU/C25A (8.28), which means that the size of the hard domain or the ordering in the hard domain increased even more for C15A nanocomposites compared to C25A nanocomposites. As shown in Table 1, the ratio of A_{NH}/A_{CH} (0.29) for ether-TPU/C15A is even lower than that of C25A (0.31) nanocomposites, while the value of A_{HCO}/A_{FCO} is 2.45, same as in C25A case. The low value of A_{NH}/A_{CH} (0.29) needs to be explained compared to C25A cases. If more urethane chains originally residing in the soft segments moved to hard domains, A_{HCO}/A_{FCO} value should have become higher than C25A case, but A_{HCO}/A_{FCO} value turned out to be the same as C25A nanocomposites. One possible explanation can be that more hydrogen bondings between −NH and ether oxygen became loose due to C15A, but not all the −NH groups released from this formed hydrogen bonding with carbonyls in the hard segments.

In Fig. 6(a), only ether-TPU/C15A exhibits the melting peak around 230 °C. Except ether-TPU/C15A, other nanocomposites do not show melting peaks around 230 °C. The melting peak around 230 °C of C15A nanocomposites shows that clay C15A promoted ordering of hard segments to form even semicrystalline region (230 °C melting) in the hard segment domain, which may be due to the fact that C15A is the most hydrophobic and the most phase separation took place in the C15A nanocomposites. In Fig. 6(a), ether-TPU/C25A exhibits onset at −58 °C which is about 14 °C higher than neat TPU and is thought to result from inclusion of clay C25A in the soft segment domains. The significant increase in this onset temperature in C25A case shows that there exists some level of affinity between the clay and soft segment polyol and again may be explained in thermodynamic sense that the balance

between the hydrophobicity of the clay resulting from modifiers and exposed silicate surface, and the level of hydrophobicity of the ether polyol. Under the same reasoning the clay C15A also is expected to be incorporated into the soft segment domains and to increase the onset temperature. But only a 3 °C increase to −68 °C was observed in DSC thermogram, which may be due to the excess aliphatic modifiers in the clay C15A. The excess low molecular weight modifiers may move freely during melt processing and thereby lower the onset temperature of polyol movement from −58 °C and also facilitate the alignment of the molecules thereby resulting in the microcrystalline region with melting point around 230 °C. One more possibility is that if excess aliphatic modifiers remain stuck together on the clay surface it will make clay surface completely hydrophobic and weaken the interaction between the clay surface and polyol resulting in little increase in the onset temperature. Analyses described so far appear to be consistent that clay C30B may form hydrogen bonding with TPUs while clays C25A and C15A are mainly incorporated into soft polyol segment domains.

3.2.2. Ester-TPU nanocomposites

Nanocomposites of ester-TPU with clays can be explained in the same context as the ether-TPU ones. One clear difference between ester-TPU and ether-TPU is that ester-TPU has carbonyl groups also in the polyol segments as well as in the urethane hard segments. Therefore, soft segment is more hydrophilic than ether polyols and more phase mixing usually takes place between the hard segments and soft segments. For ester-TPU with PM, the ratio (0.62) of A_{NH}/A_{CH} shown in Table 1 remains same as that (0.62) of pure ester-TPU. To investigate if this result means that the clay PM did not produce any effect on the ester-TPU, the DSC thermogram was also taken for ester-TPU nanocomposites as shown in Fig. 5(b) and the area under the endothermic peaks around 160 °C were shown in Table 2. The areas under 160 °C endothermic peaks for ester-TPU nanocomposites exhibit that the endothermic area (8.10) of ester-TPU/PM is larger than that (7.35) of neat ester-TPU. This means that the size of the hard domain or the ordering in the hard domain increased for ester-TPU/PM nanocomposites compared to neat ether-TPU. This is also manifested in the second-run DSC results shown in Fig. 6(b). The onset temperature of exothermic peaks for ester-TPU is shown around −61 °C, which may arise from the movement of soft segment. This temperature decreased to −78 °C for ester-TPU/PM nanocomposite, which means that phase demixing occurred by the addition of clay PM. Phase demixing promoted more ordering in the hard domains and lowering of onset temperature of soft segment movement since hard segments are demixed from the soft segment domains. This is consistent with the first-run DSC results in Table 2 where the endothermic area increased. From above results, clay PM appears to give some effect on the morphology of ester-TPU. In spite of demixing of urethane segments in soft domains, ratio of A_{NH}/A_{CH} remain same as those of neat ester-TPU. The counterpart of −NH in hydrogen bonding may be changed from ester-polyol carbonyls to urethane carbonyls in this case.

In ester-TPU/C30B, the value of A_{NH}/A_{CH} increased to 0.65 from 0.62 of pure TPU as shown in Table 1. Endothermic area for C30B nanocomposites in Table 2 shows that the ordering in the hard segment domain was reduced just slightly, which means that C30B interacted with hard segment domains a little bit. The onset temperature around −60 °C remains about the same as pure ester-TPU in Fig. 6(b) indicating that the soft segment domain was not affected much. From these observations, one possible explanation for the increase in A_{NH}/A_{CH} may be the interaction of loosened −NH of hard segments either with carbonyls of ester-polyols or with some sites of C30B. But still the possibility of hydrogen bond formation between hydroxyls of C30B and carbonyls of ester-polyols cannot be excluded completely.

In the nanocomposites of ester-TPU/C25A, the ratio of A_{NH}/A_{CH} decreased to 0.58 from 0.62 of neat ester-TPU. This decrease in ratio indicates that the hydrogen bonding between −NH and carbonyls, whether they are in the hard segments or in the soft segments, decreased by the addition of C25A. The endothermic area (7.27) of the first-run DSC result for ester-TPU/C25A shown in Table 2 remains almost same as that of neat TPU (7.35) indicating that the hard domains were not affected much. In the second-run DSC result shown in Fig. 6(b), the soft segment movement temperature appears to be −71 °C which is lower than pure TPU indicating that some phase demixing occurred. A difference between the ester-TPU nanocomposites and the ether-TPU nanocomposites is although there occurred some phase demixing in ester-TPU nanocomposites, hard domain ordering did not increase. This may be due to the intrinsic better mixing of phases in the ester-TPU case. Similar trend was observed for ester-TPU/C15A, where more decrease in A_{NH}/A_{CH} ratio was obtained. Similar reasoning may be applied for the interpretation of the results. Clay C15A interferes with the soft segments which cause the decrease in the hydrogen bonding between −NH of hard segments and carbonyls of ester-polyols in the soft segments resulting in the decrease in the A_{NH}/A_{CH} values. Decrease in the onset temperature of soft segment movement in C15A nanocomposites to −68 °C which is lower than pure ester-TPU shows the effect of C15A on the soft segments. Little decrease in the endothermic area (7.05) in this case compared to neat ester-TPU (7.35) indicates that not much ordering in the hard segments occurred and accordingly no melting peak around 230 °C was observed in Fig. 6(b) for the ester-TPU/C15A nanocomposites which is different from ether-TPU/C15A.

All the above analyses were made based on the assumption that the thermal degradation of TPU nanocomposites was not serious enough to affect the FTIR or DSC results, which is thought to be the case since the mechanical properties of the nanocomposites after the first processing were fairly good for all the nanocomposites. Above FTIR results were obtained with the first-extrusion samples.

3.3. Tensile properties

The stress–strain curves from tensile tests of ether- and ester-TPU/clay nanocomposites along with neat TPUs are

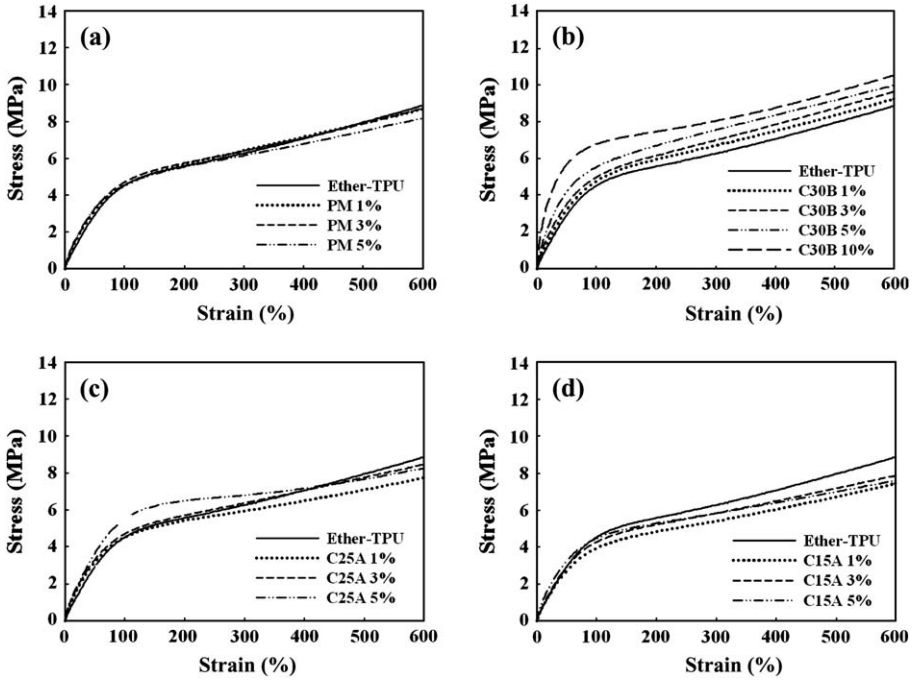

Fig. 7. Tensile stress–strain curves of ether-TPU nanocomposites with (a) PM, (b) C30B, (c) C25A and (d) C15A at different clay loadings.

shown in Figs. 7 and 8, respectively and the corresponding tensile properties are summarized in Table 3.

For ether-TPU nanocomposites, the C30B nanocomposite shows the best improvement in tensile modulus and stress at 500% strain (Fig. 7(b)) among the various clays added. Highest improvement in the tensile properties of nanocomposites with C30B can be attributed to the good dispersion of exfoliated silicate layers. Especially, the degree of improvement increases with increasing clay contents, which may be the another indirect evidence of interaction between C30B and ether-TPUs. The stresses at 500% strain for C25A, C15A and PM nanocomposites in Table 3 are shown to be lower than neat ether-TPU although a small increase in modulus was observed. Increase in modulus is not uncommon for polymeric composites even without notable interfacial attraction between matrix polymers and inorganic fillers.

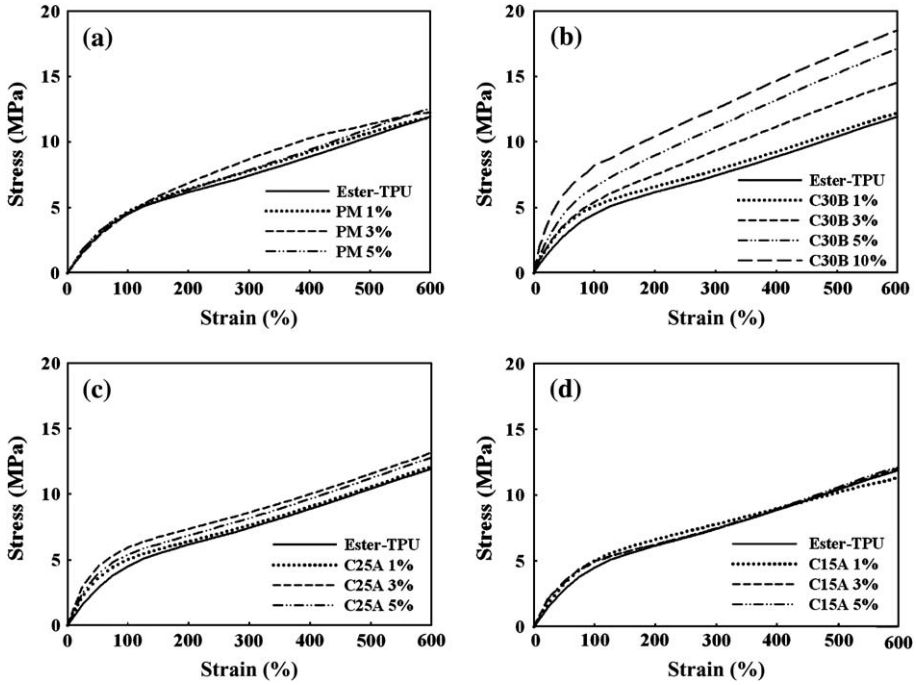

Fig. 8. Tensile stress–strain curves of ester-TPU nanocomposites with (a) PM, (b) C30B, (c) C25A and (d) C15A at different clay loadings.

Table 3
Tensile properties of TPU nanocomposites

Sample	Ether-TPU		Ester-TPU	
	Tensile modulus (MPa)	Stress at 500% strain (MPa)	Tensile modulus (MPa)	Stress at 500% strain (MPa)
TPU	6.2	8.2	6.4	10.4
TPU/PM				
1 wt%	6.9	8.3	6.5	10.3
3 wt%	6.8	7.7	7.2	11.2
5 wt%	7.4	7.6	7.1	10.9
TPU/C30B				
1 wt%	8.5	8.4	8.1	10.5
3 wt%	8.9	8.8	8.1	12.5
5 wt%	9.8	9.1	10.7	15.8
10 wt%	14.2	9.8	14.6	16.2
TPU/C25A				
1 wt%	7.0	7.2	8.3	10.5
3 wt%	7.0	7.7	10.1	11.4
5 wt%	7.2	7.4	8.9	11.3
TPU/C15A				
1 wt%	6.4	7.1	6.5	10.2
3 wt%	6.7	7.2	6.6	10.6
5 wt%	7.3	6.7	7.2	10.5

A decrease in stress at 500% strain for PM nanocomposite may be from the poor dispersion of PM in the nanocomposites and the decrease observed for ether-TPU/C25A or C15A is believed to be due to the low-molecular-weight organic modifiers in those clays.

In ester-TPU nanocomposites, both the tensile modulus and the stress at 500% strain of ester-TPU with 10 wt% of C30B significantly increased more than 100% and 50%, respectively over those of neat TPUs as shown in Fig. 8(b) and Table 3. The ester-TPU nanocomposites containing C25A (Fig. 8(c)) also exhibit increase in both tensile modulus and stress at 500% strain over the neat ester-TPU, but to a less extent than C30B nanocomposites. For the ester-TPU nanocomposites with C15A shown in Fig. 8(d), little improvement in both properties was observed compared to neat ester-TPU, with small improvement in only the tensile modulus at low strain, which may be again due to the excess of organic modifiers in the clay C15A. In ester-TPU/PM, stress at 500% strain remains around the same as neat ester-TPU while only a slight increase in modulus was observed.

These tensile test results again coincide with the TEM, XRD and FTIR results, where C30B shows the best dispersion of clay followed by C25A and C15A. As can be seen from Table 3, tensile properties of ester-TPU nanocomposites are generally higher than those of ether-TPU nanocomposites. This is somewhat different from what is expected in view of TEM results where ether-TPU nanocomposites showed better dispersion of clays. This may be partly due to the higher viscosity of ester-TPU than ether-TPU as shown in Section 3.4 and also partly due to the morphological differences as described in Section 3.2. One more possibility is that the clay located in the soft segment domain may interact with the carbonyls of ester-polyol in the case of ester-TPU nanocomposites.

Since it was known that the organic modifiers in the clays start to degrade around 200 °C and also the clays can accelerate the degradation of TPU, the second extrusion samples of TPU/clay 30B nanocomposites were prepared by extruding the TPU and clay twice in the extruder by refeeding the first extrudate again into the twin screw extruder.

Tensile test results for ether- and ester-TPU after the second extrusion are shown in Fig. 9(a) and (b). Considerable drop in tensile properties compared to the first-extrusion sample was observed as can be seen in the figures. Especially, a largest drop was observed for nanocomposites containing 10 wt% C30B indicating that the clay was involved in lowering tensile properties. Slight color formation in the sample was observed after the second extrusion. Since the color change was very weak, degradation does not seem to be the sole cause of decrease in the tensile properties and consideration should be given to the possibility that the change in morphology of nanocomposites by exposing the nanocomposites to extended shear in two-time extrusion may do some roles in determining the tensile properties. This result shows that too long residence time in the extruder can lower the mechanical properties of TPU/clay nanocomposites.

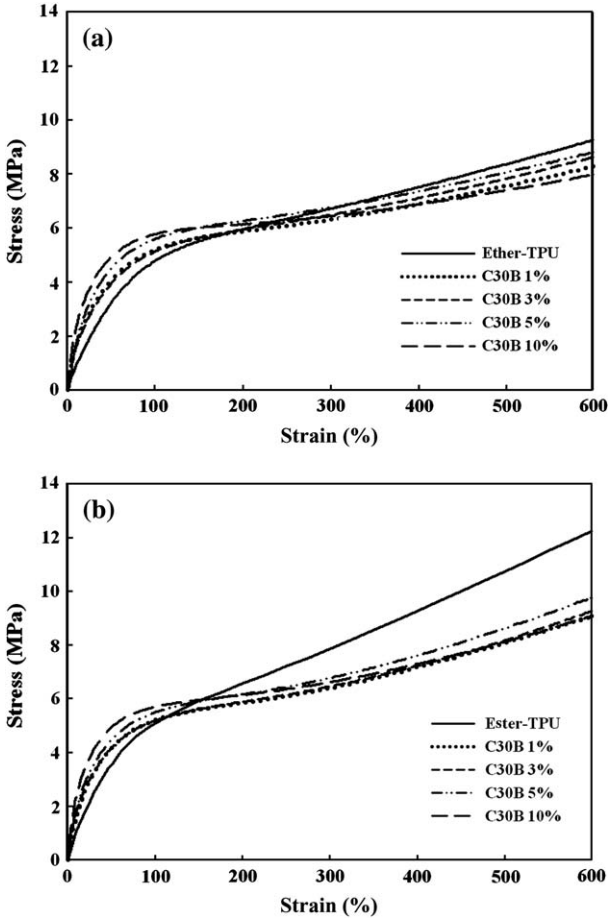

Fig. 9. Tensile stress–strain curves of (a) ether-TPU nanocomposites and (b) ester-TPU nanocomposites with various compositions of C30B after the second extrusion.

3.4. Rheological properties' measurements

The plot of complex viscosity η^* vs frequency ω and the plot of G' vs G'' for ether-TPU without and with clays PM, C30B, C25A and C15A are shown in Fig. 10(a) and (b). Neat ether-TPU and ether-TPU/PM exhibited the similar behavior as shown in Fig. 10(a), where they showed almost Newtonian behavior with little change in complex viscosity at varying frequencies, while those with C30B, C25A or C15A exhibited higher slopes indicating a shear thinning behavior. Shear thinning behavior with higher slope for better clay dispersion was previously observed for other nanocomposites in the literature [35]. This means that the dispersion of clay in nanocomposites with C30B, C25A or C15A is better than those with PM. In Fig. 10(b) showing G' vs G'', pure ether-TPU and nanocomposites with PM again show a similar behavior, while those with C25A, C15A and C30B showed higher slopes showing different behaviors. Higher slopes in plots of G' vs G'' was attributed to the enhanced dispersion of clays in the previous study though different polymers were used in that study [36].

Fig. 11(a) and (b) shows the plot of complex viscosity η^* vs frequency ω and the plot of G' vs G'', respectively, for ester-TPU without and with clays. Similar trend with ether-TPU nanocomposites were observed again indicating the dispersed clay structure for C30B, C25A and C15A nanocomposites.

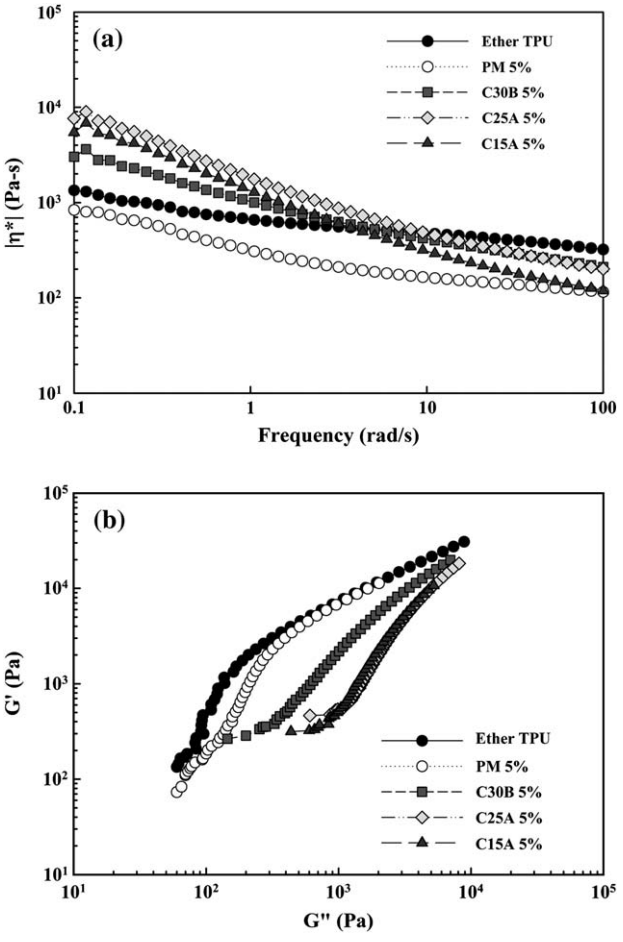

Fig. 10. (a) Complex viscosity (η^*) vs frequency (ω) and (b) G' vs $G''$of ether-TPU nanocomposites at 5 wt% clay loading.

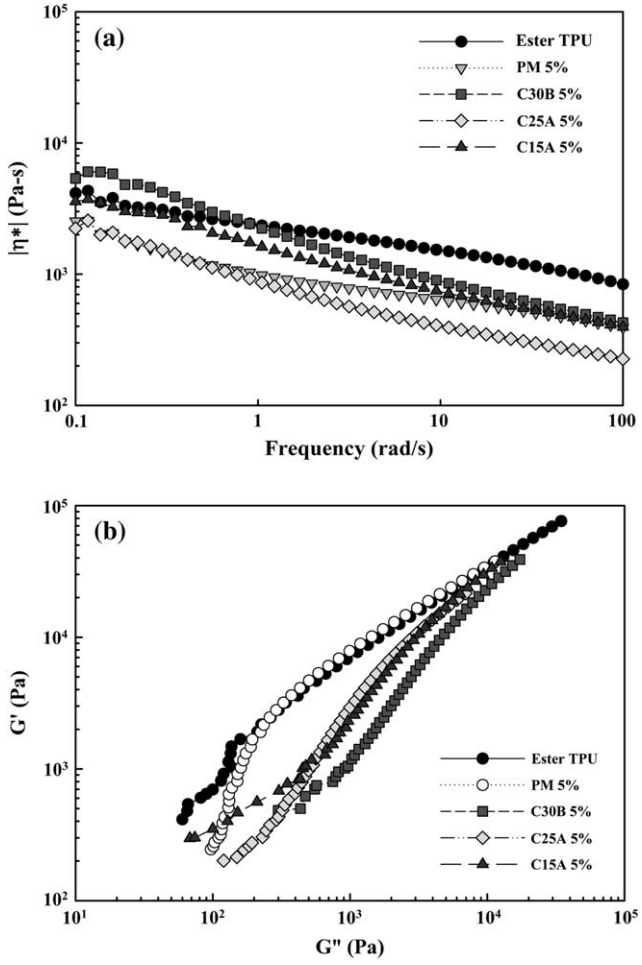

Fig. 11. (a) Complex viscosity (η^*) vs frequency (ω) and (b) G' vs $G''$of ester-TPU nanocomposites at 5 wt% clay loading.

4. Conclusions

Ether- and ester-TPUs/clay nanocomposites were prepared by melt compounding using various types of clays. In the case of nanocomposites with clay C30B, TEM images show a very good dispersion of clays close to exfoliation in both ether- and ester-TPU nanocomposites. Ether- and ester-TPU/C25A or C15A nanocomposites display the partially intercalated structures as revealed by XRD and TEM. Areas under −NH or carbonyl peaks in FTIR spectra and areas under endothermic peaks and the onset temperature of soft segment movement in DSC thermograms were analyzed to study the change in the morphology of nanocomposites. These analyses indicate that C30B may be involved in the interaction with ether- or ester-TPUs and clay C25A may induce the demixing of hard and soft segments. Decrease in the onset temperature of soft segment movement in ester-TPU/C15A nanocomposites compared to pure ester-TPU exhibits the effect of C15A on the soft segments. Differences in the area under −NH and carbonyl

peaks in FTIR spectra for all nanocomposites were analyzed in conjunction with the corresponding DSC results.

In the TEM images, ether-TPU-based TPU nanocomposites exhibit better dispersion of clays than ester-TPU ones while the tensile properties show the opposite trend. The tensile properties of ether- or ester-TPU nanocomposites with C30B showed the highest improvement compared to the ones with other clays. Although the improvement in tensile properties decreased after the second extrusion of the nanocomposites, properties of the nanocomposite after first melt processing were still good enough for practical applications.

Acknowledgements

This study was supported by the Center for Environmental and Clean Technologies designated by MOCIE in The University of Suwon. We acknowledge the efforts of the Korea Basic Science Institute for taking very nice TEM pictures.

References

[1] Hepburn C. Polyurethane elastomers. 2nd ed. London: Elsevier Science Publishers; 1992 [chapter 9].
[2] Oertel G. Polyurethane handbook. 2nd ed. Munich: Carl hanser; 1993. p. 465–74.
[3] Wang CB, Cooper SL. Macromolecules 1983;16:775–86.
[4] Hu CB, Ward Jr RS, Schneider NS. J Appl Polym Sci 1982;27:2167–77.
[5] Martin DJ, Meijs GF, Renwick GM, McCarthy SJ, Gunatillake PA. J Appl Polym Sci 1996;62:1377–86.
[6] Chen TK, Tien YI, Wei KH. Polymer 2000;41:1345–53.
[7] Kojima Y, Usuki A, Kawasumi M, Okada A, Fukushima Y, Kurauchi T, et al. J Mater Res 1993;8:1179–84.
[8] Vaia RA, Jandt KD, Kramer EJ, Giannelis EP. Macromolecules 1995; 28:8080–5.
[9] Krishnamoorti R, Giannelis EP. Macromolecules 1997;30:4097–102.
[10] Vaia RA, Giannelis EP. Macromolecules 1997;30:8000–9.
[11] Wang MS, Pinnavaia TJ. Chem Mater 1994;6:468–74.
[12] Vaia RA, Ishii H, Giannelis EP. Chem Mater 1993;5:1694–6.
[13] Chiu FC, Lai SM, Chen JW, Chu PH. J Polym Sci Part B Polym Phys 2004;42:4139–50.
[14] Lee KM, Han CD. Polymer 2003;44:4573–88.
[15] Lee SS, Kim JK. J Polym Sci Part B Polym Phys 2004;42:246–52.
[16] Loyens W, Jannasch P, Maurer FHJ. Polymer 2005;46:903–14.
[17] Choi WM, Kim TW, Park OO, Chang YK, Lee JW. J Appl Polym Sci 2003;90:525–9.
[18] Solarski S, Bernali S, Rochery M, Devaux E, Alexandre M, Monteverde F, et al. J Appl Polym Sci 2005;95:238–44.
[19] Varghese S, Gatos KG, Apostolov AA, Karger-Kocsis J. J Appl Polym Sci 2004;92:543–51.
[20] Rhoney I, Brown S, Hudson NE, Pethrick RA. J Appl Polym Sci 2004;91:1335–43.
[21] Tortora M, Gorrasi G, Vittoria V, Galli G, Ritrovati S, Chiellini E. Polymer 2002;43:6147–57.
[22] Tien YI, Wei KH. J Appl Polym Sci 2002;86:1741–8.
[23] Chang JH, An YU. J Polym Sci Part B Polym Phys 2002;40:670–7.
[24] Han B, Cheng A, Ji G, Wu S, Shen J. J Appl Polym Sci 2004;91: 2536–42.
[25] Pattanayak A, Jana SC. Polymer 2005;46:3275–88.
[26] Pattanayak A, Jana SC. Polymer 2005;46:3394–406.
[27] Pattanayak A, Jana SC. Polymer 2005;46:5183–93.
[28] Finnigan B, Martin DJ, Halley P, Truss R, Campbell K. Polymer 2004;45:2249–60.
[29] Fornes TD, Hunter DL, Paul DR. Macromolecules 2004;37:1793.
[30] Jang BN, Wang D, Wilkie CA. Macromolecules 2005;38:6533–43.
[31] Tanaka G, Goettler LA. Polymer 2002;43:541–53.
[32] Xie W, Gao Z, Pan W-P, Hunter D, Singh A, Vaia R. Chem Mater 2001;13:2979–90.
[33] Hummel DO. Atlas of polymer and plastics analysis. 3rd ed. Munich: Hanser Publishers; 1991.
[34] Srichatrapimuk VW, Cooper SL. J Macromol Sci Phys 1978;B15(2): 267–311.
[35] Lee KM, Han CD. Macromolecules 2003;36:804–15.
[36] Choi S, Lee KM, Han CD. Macromolecules 2004;37:7649–62.